Chapter 6

Photonic Crystals

6.1 Introduction

Photonic crystals (PCs) are optical materials [1, 2] with periodic changes in the dielectric constant on the wavelength scale, in which forbidden propagation frequency ranges called photonic bandgaps (PBGs) can be created for certain ranges of photon energies. In PCs, we can describe photons in terms of a band structure, as in the case of electrons. Depending on the dimensions of the periodic array, 1D, 2D, and 3D PCs can be realized. A dielectric Bragg mirror, which is well known for many different applications, is an example of 1D PC. In Fig. 6.1, the 1D, 2D, and 3D PC structures created by intersecting two different materials with high and low refractive indexes are presented.

Light of frequencies corresponding to PBG cannot be transmitted in a PC except when defects are introduced. If a defect is included in the PBG structure, a state can be formed in the gap. This state is analogous to a defect or impurity state in a semiconductor that forms a level within the semiconductor bandgap. Defects in PBG structures are engineered by incorporating breaks in the periodicity of the PBG device. A break in periodicity leads to a defect state whose shapes and properties would be dictated by the defect's nature.

Silicon-Based Photonics
Erich Kasper and Jinzhong Yu

ISBN 978-981-4303-24-8 (Hardcover), 978-1-315-15651-4 (eBook)
www.jennystanford.com

A defect in a PC could, in principle, be designed to be of any size, shape, or form and could be chosen to have any of a wide variety of dielectric constants. Thus, defect states in the gap could be tuned to any frequency and spatial extent of design interest.

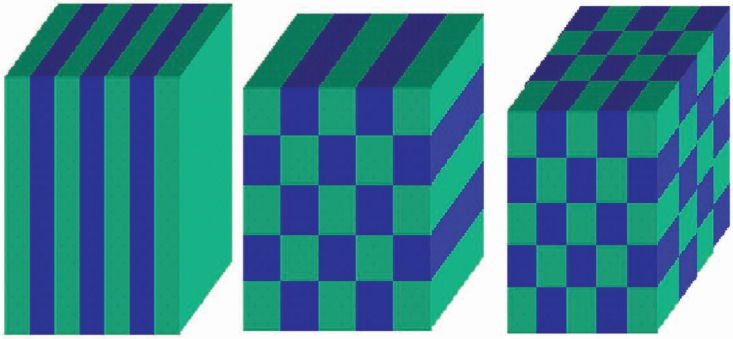

Figure 6.1 1D, 2D, and 3D PCs by alternating of refractive index in corresponding dimensions.

A PC being a kind of artificial material, its properties depend on the physical characteristics of the elementary materials that go into its construction. In this case, silicon shows a lot of advantages in realizing PC structures in the following two aspects: firstly, the index contrast between silicon and silica or air is very large, which is vital to a PC because a large enough index modulation is the premise of creating a wide enough PBG. Second, the feature size of a PC is on the order of wavelength, which means we need to fabricate an index-modulated structure comparable to the working wavelength, which is not a problem when using mature silicon-based processes. Therefore, silicon PC possesses theoretical and real possibilities to discover and apply excellent and special photonic effects of PC on subwavelength and nanoscale, which has made it a hot research topic within the last decades, and a lot of novel and high-performance devices and circuits have been created based on silicon PC.

Ideally, a complete PBG exists in a 3D PC. However, due to the difficulty of 3D fabrication to date, most of the experimental research and breakthrough in silicon-based PCs is based on 2D PCs. In the following parts, we are focusing on the simulation, fabrication, and characterization of silicon-based PC slabs owing to the said reason.

6.2 Master Equation

Maxwell's equations have been employed to analyze such periodic structures. In mks units, we have:

$$\begin{aligned} &\nabla \times \vec{D} \rho \\ &\nabla \times \vec{D} = 0 \\ &\nabla \times \vec{E} = -\frac{\partial \vec{B}}{\partial t} \\ &\nabla \times \vec{H} = \frac{\partial \vec{D}}{\partial t} + \vec{j} \end{aligned} \tag{6.1}$$

Here $\vec{E}$ and $\vec{H}$ are electric and magnetic fields, $\vec{D}$ and $\vec{B}$ are displacement and magnetic induction fields, and it is assumed that free charges and electric current are absent.

For linear, lossless, and isotropic dielectric materials, the following relationships are well known: the electric field and the displacement can be related by Eq. 6.2:

$$\begin{aligned} \vec{D} &= \varepsilon_0 \varepsilon \vec{E} \\ \vec{B} &= \mu_0 \mu \vec{H} \end{aligned} \tag{6.2}$$

Here ε and ε_0 are the dielectric constants of the PC material and free space, respectively and μ and μ_0 are the magnetic permeability of the PC material and free space, respectively. For most of the PC materials of interest, $\mu = 1$ and $p = j = 0$.

By substituting Eq. 6.2 into Eq. 6.1, Maxwell's equations become a group of linear equations. $\vec{E}$ and $\vec{H}$ can be written as harmonic modes, and the time and spatial dependence of $\vec{E}$ and $\vec{H}$ can be separated.

$$\begin{aligned} \vec{H}(r,t) &= \vec{H}(r) e^{-i\omega t} \\ \vec{E}(r,t) &= \vec{E}(r) e^{-i\omega t} \end{aligned} \tag{6.3}$$

The following equation can be obtained [3] by substituting Eq. 6.3 into Eq. 6.1:

$$\Delta \times \left(\frac{1}{\varepsilon(r)} \Delta \times \vec{H}(r) \right) = \left(\frac{\omega}{c} \right)^2 \vec{H}(r) \tag{6.4}$$

Here c is the velocity of light in free space ($c = 1/\varepsilon_0 \mu_0$). Equation 6.4 is called the master equation of a PC giving out the distributions of magnetic field $\vec{H}(r)$ at the corresponding frequency ω.

6.3 Calculation Methods

6.3.1 PWE Method

For a PC structure with a periodic dielectric material array, the electromagnetic modes have to satisfy not only the master equation but also a periodic condition. Because of the periodicity of a PC structure, the PC material system is unchanged for the translation along the direction of the periodic array, which is called a translational symmetry system and d denotes the lattice vector. Electromagnetic modes for a translational symmetry system [4] can be written in a "Bloch form." In this case, Eq. 6.4 can be expanded with a group of planar waves.

Hence, bandgap maps and the inside optical field can be calculated by using Bloch theory to solve Maxwell's equations with a periodic dielectric distribution.

As an example, we calculate the PBG of a silicon-on-insulator (SOI) PC slab with t = 0.5a and r = 0.38a, where a, r, and t represent the lattice constant of PC, the radius of air holes, and the thickness of the top silicon waveguide layer, respectively. The result is illustrated in Fig. 6.2. It is seen that for transverse electric (TE)-like modes, the PBG is from a normalized frequency of 0.3078 to 0.4415 and there

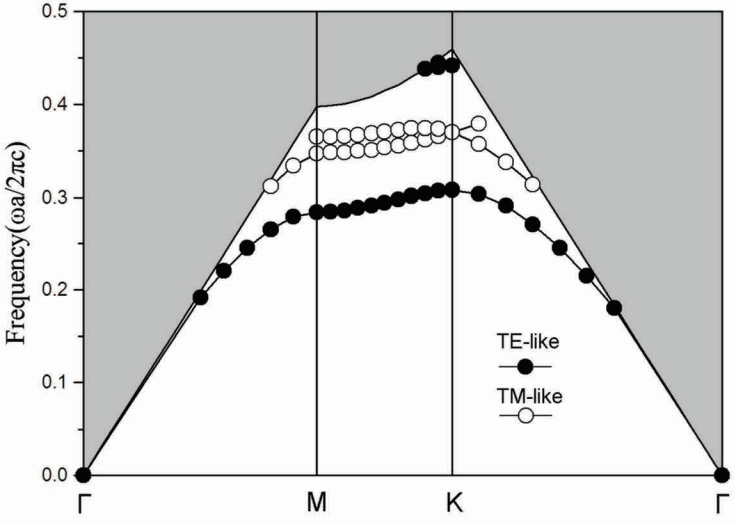

Figure 6.2 Calculation of an SOI PC slab with PWE.

is no PBG for transverse magnetic (TM)-like modes. Therefore, if the center wavelength is 1.3 μm, then a = 480 nm, r = 182.4 nm, and t = 240 nm are proper dimensions of the PC. The calculated bandgap corresponds to the wavelength range of 1087 nm to 1559 nm, which is wide enough for fiber communication applications.

However, what has to be clarified here is that the above planar wave expansion (PWE) method suitable for the perfect PC structure should be modified for PC structures with defects, because a lot of photonic effects are only meaningful in a PC structure with defects. For the simulation of such structures, we need to use the so-called supercell method. And the point is that the supercell but not the original Bragg cell constructs the whole crystal. For example, if we want to calculate a PC line defect waveguide as shown in Fig. 6.3a, the rectangular region that contains the repeatable defect structure is taken as the supercell used in calculation instead of the original square cell. And in the reciprocal lattice, the range of the first Brillouin zone changes from YMX to Y'M'X'. Detailed theoretical methods and considerations to calculate PC modes using the PWE are available in the literature.

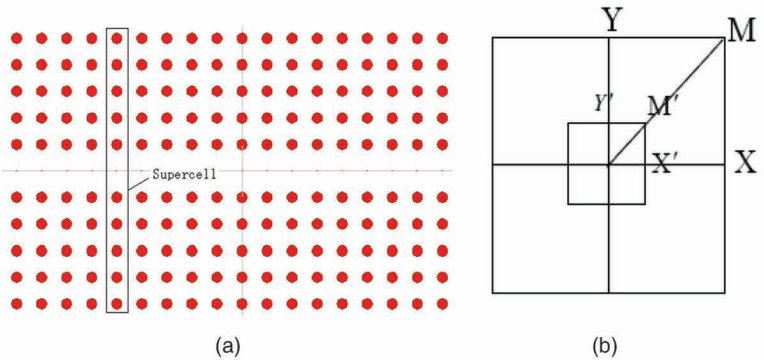

Figure 6.3 (a) The supercell used in the calculation of the PC line defect waveguide. (b) YMX and Y'M'X' correspond to the first Brillouin zone of the original Bragg cell and supercell.

6.3.2 FDTD Method

A finite difference time domain (FDTD) method solves Maxwell's equations numerically [5, 6].

The derivatives in the above equations are approximated by finite differences and the electromagnetic field components are located on a Yee cell. For 2D FDTD, the electric field components at time $n\Delta t$ are located on the sides of the Yee cell while the magnetic field components at times $(n + 1/2)\Delta t$ are located at the center of the Yee cell, as shown in Fig. 6.4 for TE mode.

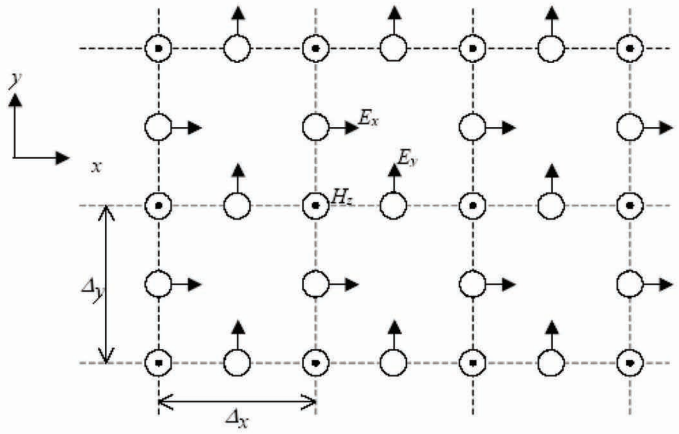

Figure 6.4 Yee cell used in FDTD for TE mode.

Two other problems should be taken into account when using FDTD. One is the algorithm stability. The Courant condition should be satisfied in order to avoid numerical instability. For a given grid size, the time step should be less than a certain value given by the Courant condition. The grid size used for a simulation should be small enough to resolve the smallest feature in the fields and structure during a simulation.

The other problem is the boundary condition. The boundary conditions at the spatial edges of the computational domain must be carefully considered. Many simulations employ an absorbing boundary condition that eliminates any outward propagating energy that impinges on the domain boundaries. One of the most effective is the perfectly matched layer (PML), in which both electric and magnetic conductivities are introduced in such a way that the wave impedance remains constant, absorbing the energy without inducing reflections. In other words, a PML boundary, which

consists of several points at the edge of the domain, is designed to act as a highly lossy material, which absorbs all incident energy without producing reflections. This allows field energy that hits the boundary to effectively leave the domain.

6.4 Silicon-Based PC Slab

6.4.1 Important Points about the SOI PC Slab

In a pure 2D PC, the electric field of TM polarization is along the axes air hole or dielectric rods forming PC and the electric field of TE polarization is perpendicular to that of the TM counterpart. However, in a quasi-2D structure, for example, a PC slab as shown in Fig. 6.5, because of alternation of EM boundary conditions and breakage in symmetry, we cannot get pure TE or TM modes but TE-like or TM-like modes with a part of electric fields in other directions. In this case, there may only be a bandgap in one symmetry/polarization and the coupling of TE-like and TM-like modes may lead to extra loss in PC devices.

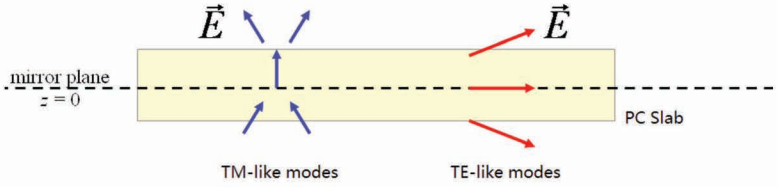

Figure 6.5 Symmetry in a PC slab.

Calculation shows that for a PC slab constructed by dielectric rods in air, a PBG exists only for TM-like polarization. And for a PC slab constructed by air holes in dielectric material, a PBG exists only for TE-like polarization. Considering the coupling loss to air for an air hole PC is smaller than for a rod PC, the former is used more often to design and fabricate devices.

To realize an air hole PC structure in an SOI wafer, normally four structures can be fabricated as shown in Fig. 6.6. Figure 6.6a is the basic structure, which is the easiest to fabricate. However, because of an asymmetric structure (air/Si/SiO_2), TE-like mode

and TM-like mode are much easier to couple, leading to a larger loss in waveguides and microcavities. If we etch the air holes down to buried SiO_2 on the basis of Fig. 6.6a, the coupling loss can be made less and the PBG becomes wider owing to a larger effective index contrast between core and cladding. To get a symmetric structure, we can either remove the buried SiO_2 to form an PC air-bridge (Fig. 6.6b) or deposit a layer of SiO_2 on top of the original structure. The air-bridge has the best optical performance, but it is complicated in process and easy to collapse. The last structure is also symmetric, but the refractive index contrast between Si and SiO_2 is less than that between Si and air and the resulting PBG is narrower. And the quality of coated SiO_2 also affects device performance. No matter which kind of PC structure of Fig 6.6 is adopted, the thickness of the core should be less than the single-mode height of the same sandwiched planar waveguide since vertical confinement is achieved by index contrast as discussed above and there is a certain value of core thickness for achieving the widest PBG for all structures.

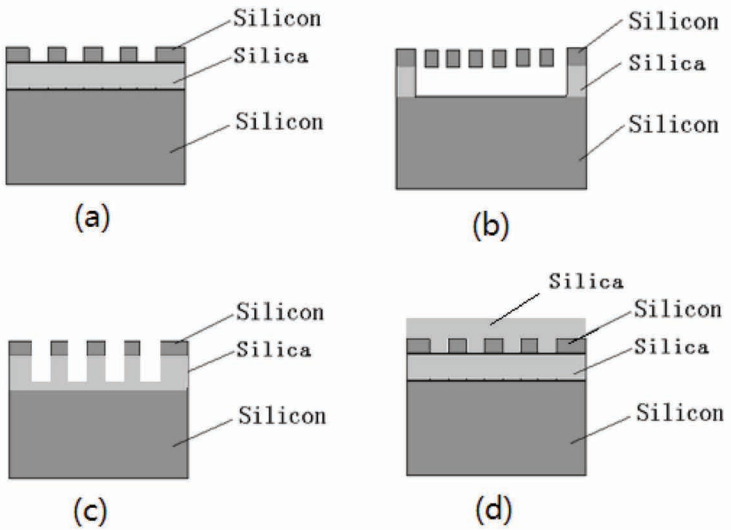

Figure 6.6 Four different PC structures in an SOI slab: (a) asymmetric slab, (b) air-bridge, (c) deep-etched asymmetric slab, and (d) symmetric slab with SiO_2 coated.

6.4.2 Fabrication of Silicon-Based PC Slab

For the fabrication [7] of 1D or 2D PCs, normally micro- or nanofabrication techniques are used. The basic process flow is listed in Fig. 6.7 and Table 6.1, taking the fabrication of an SOI-based passive PC structure as an example. Given an SOI wafer, first we need to clean it thoroughly to avoid the influence of contaminations on device performance. Then photoresist is spun-on in order to "record" optical lithography or the e-beam lithography result. Since typical dimensions of near-infrared or mid-infrared PCs are about 500 nm, deep UV lithography or e-beam lithography is often used to get higher precision. The thicker the photoresist, the lower the resolution will be in lithography, but the etch ratio of resist over silicon in the followed etching process should be considered when a resist thickness is selected. Before lithography, the resist needs baking to vaporize the solvent. Then lithography and development are done to define the structure in the resist, followed by another baking called "postbake" to drive off the developing solution and to harden the resist for etching. The purpose of etching is to transfer the structure from resist to wafer, and inductively coupled plasma (ICP) or reactive-ion dry etching method is mostly used for silicon. The last step is to remove the resist from the wafer after etching, using oxygen plasma or acetone.

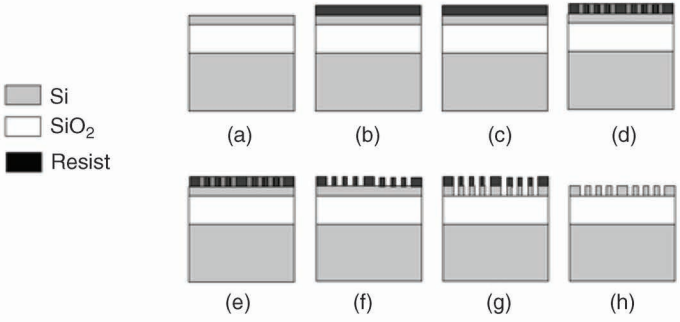

Figure 6.7 Fabrication of SOI passive PC structures [7]: (a) wafer cleaning, (b) resist spin-on, (c) prebake, (d) lithography (e) development, (f) postbake, (g) etching, and (h) resist removing.

Table 6.1 Example of a process flow for the fabrication of SOI passive PC structures

No.	Process	Purpose	Recipe/description
(a)	Wafer cleaning	To avoid deterioration of structure owing to contamination	1. Acetone bath (10 min. ultrasonic) 2. Methanol bath (5 min. ultrasonic) 3. Deionized water (DI) rinse 4. RCA clean (H_2O:NH_4OH:H_2O_2 = 5:1:1) 5. DI rinse 6. HF dip 7. DI rinse and blow dry (N_2)
(b)	Resist spin-on	To prepare a film to "record" the lithography result	1. Material: 950 K PMMA C_2 2. Parameters: spin-coated at 3000 rpm 3. Result: thickness ≈ 150 nm
(c)	Prebake	To vaporize solvent of resist	On a hotplate at 180°C for 10 min.
(d)	Lithography	To define structure in resist	1. Acceleration voltage: 10 kV (e-beam) 2. Aperture: 30 μm 3. Area dose: 70 μA s/cm^2
(e)	Development	To present structure in resist	1. Developed in MIBK:IPA = 1:3 for 15 s 2. Rinsed by IPA for 15 s 3. Blow dry (N_2)
(f)	Postbake	To drive off developing solution and harden resist for etching	On a hotplate at 90°C for 4 min.
(g)	Etching	To transfer the defined structure from resist to substrate	1. Pressure = 1.6 Pa 2. SF6 flow = 60 sccm 3. C4F8 flow = 65 sccm 4. ICP power = 800 W 5. RF power = 50 W
(h)	Resist removing	To obtain the structure ready to be measured	Oxygen plasma under power 300 W or soaking the sample in acetone

Two different samples fabricated with e-beam lithography and ICP etching are shown in Fig. 6.8. Figure 6.8a is an SOI asymmetric PC slab, and Fig. 6.8b is an SOI air-bridge, in which the buried silica is removed with HF solution.

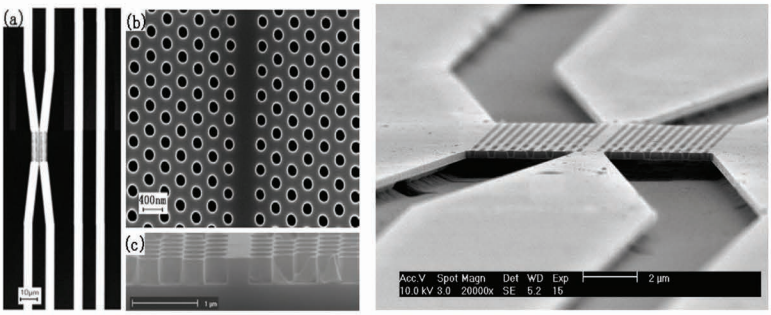

(a) (b)

Figure 6.8 (a) SOI PC waveguides in an asymmetric slab and (b) air-bridge.

6.5 SOI PC Devices

6.5.1 SOI PC Waveguides

As a channel of light transmission, an optical waveguide is the basic structure in integrated optics. By making a line defect, we can create an extended mode that we can use to guide light. Traditionally, we achieve waveguiding in dielectric structures, such as optical fibers, by total internal reflection. When the fibers are bent very tightly, however, the angle of incidence becomes too large for total internal reflection to occur and light escapes at the bend. PCs can be designed to confine light even around tight corners because they do not rely on the angle of incidence for confinement.

To illustrate this point, we remove a row of air holes from the PC described earlier. This introduces a defect-guided-mode band inside the gap. The field associated with the guided mode is strongly confined in the vicinity of the defect and decays exponentially in the crystal. An intriguing aspect of PC waveguides is that they provide a unique way to guide optical light, tractably and efficiently, through narrow channels of air. Once light is introduced inside the waveguide, it has nowhere else to go. The only source of loss is reflection from the waveguide input, which suggests that we might use PCs to guide

light around tight corners, as in Fig. 6.9. Although the bend radius of curvature is less than the light wavelength, nearly all the light is transmitted through the bend over a wide range of frequencies in the gap. The small fraction of light that is not transmitted is reflected. For specific frequencies, we can achieve 100% transmission.

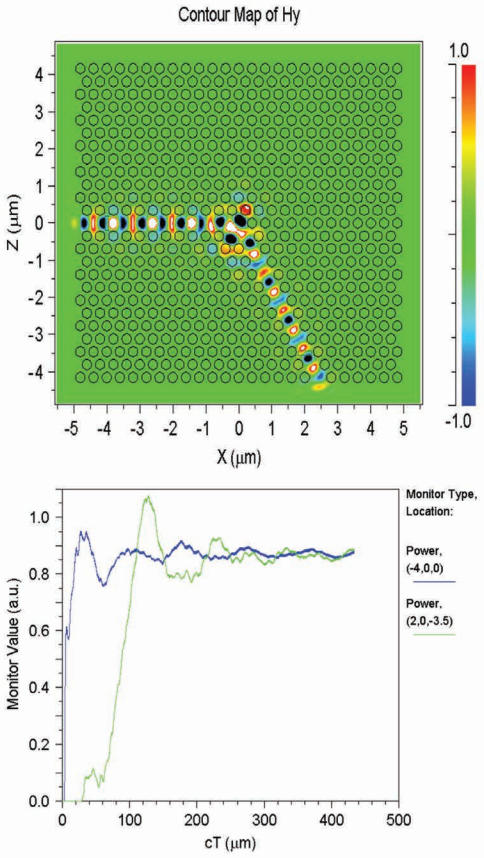

Figure 6.9 An Hy pattern in the vicinity of a sharp 120° bend. The electric field is polarized along the axis of the dielectric rods. The green circles indicate the rod position. Unlike the mechanism of total internal reflection, a PC allows light to be guided in air.

A typical PC line defect waveguide in an SOI slab with transmission characteristics is shown in Fig. 6.10. The air hole radius and periodicity are 135 nm and 410 nm, respectively, fabricated in an SOI slab with a core thickness of 240 nm. It is seen that the stop-band appears at the

wavelength of 1590 nm. And for wavelengths longer than this value, PC modes cannot be transmitted, but refractive index-guided modes still exist, so a bit higher transmission is observed as shown in Fig. 6.10.

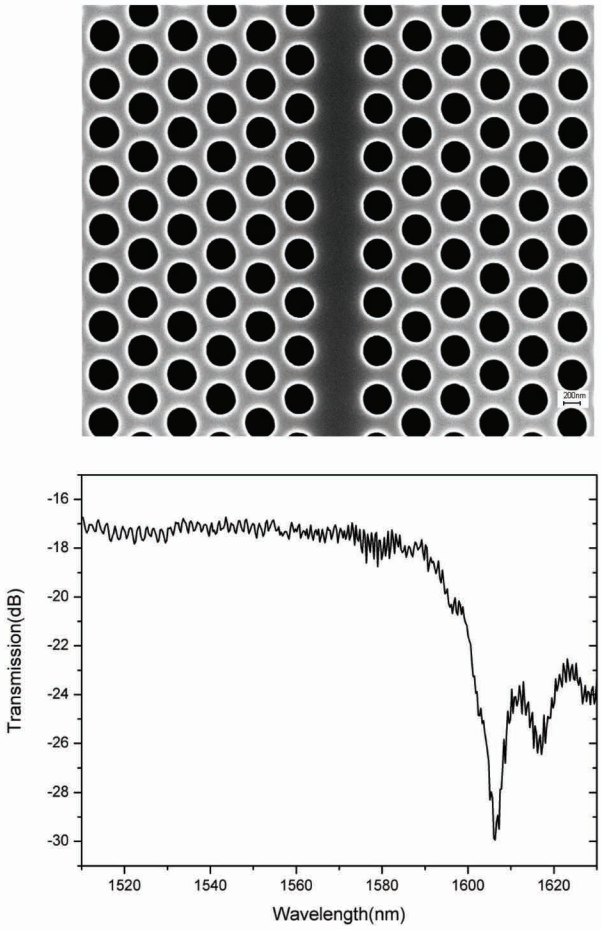

Figure 6.10 PC line defect waveguide in an SOI slab and its transmission characteristics.

6.5.2 SOI PC Microcavities

Electromagnetic resonant cavities [8], which trap light within a finite volume, are an essential component of many important optical devices and effects, from lasers to filters to single-photon sources.

Cavities are characterized by two main quantities: the modal volume V and the quality factor Q. In many applications, high Qs and small Vs are highly desirable for the high finesse required for laser and filter applications and for the high Purcell factor required for controlling the spontaneous emission of atoms placed in resonance with the microcavity mode. The control of spontaneous emission is of interest for increasing the light output and narrowing the linewidth of light-emitting diode structures and for reducing the lasing threshold of semiconductor lasers.

Figure 6.11 illustrates a sample single-defect microcavity in an SOI PC slab together with its resonant spectrum and electric field distribution. Here the air hole radius and periodicity of the triangular

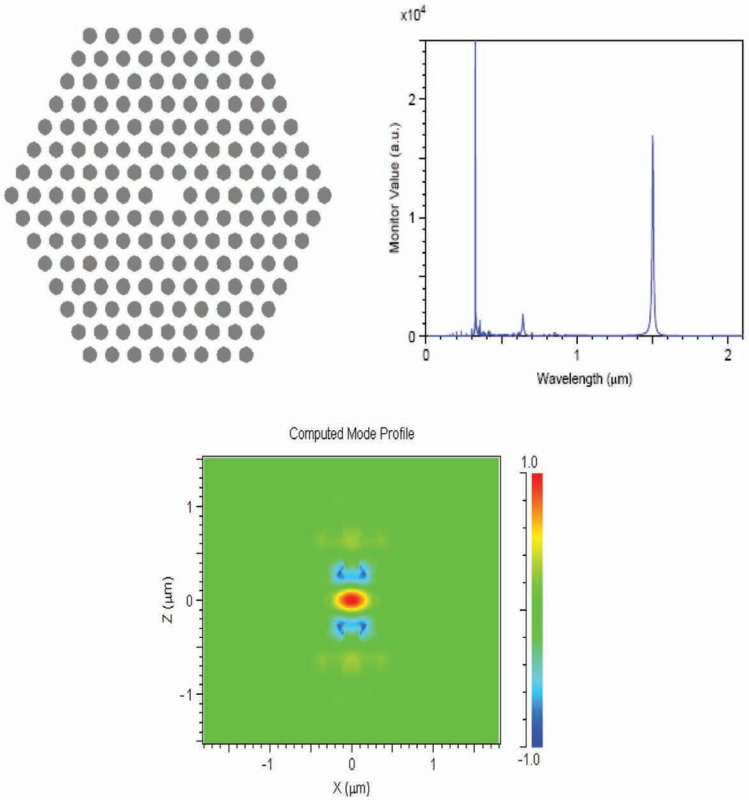

Figure 6.11 Single-dot defect microcavity in an SOI slab and its resonant spectrum and electric field distribution.

lattice are 126 nm and 420 nm, respectively, and the 3D FDTD method with X, Y, and Z step sizes of 30, 10, and 30 nm, respectively, is used for simulation. It is seen that a strong resonant mode at 1550 nm appears inside the PBG and most of the energy is well confined in the dot defect with one air hole removed.

A variety of passive and active optical photonic crystal microcavities have been constructed. It has been shown experimentally and numerically that fine-tuning of the geometry of the holes surrounding the cavity defect may drastically increase the cavity Q/V factor. Many interesting concepts have been used for optimizing the quality factors of the PC microcavities, including symmetry arguments, cancelation of the multipole far-field radiation [9], Bloch wave engineering for increasing the modal reflectivity, and more recently "gently confining" light to avoid radiation. With mature PC microcavities theory and an advanced fabrication process, the experimental Q factor (Table 6.2 [8–12]) of silicon-based PC microcavity got boosted within a decade by a factor of 10,000 and the simulated Q value exceeded 10^7.

Table 6.2 Progress of silicon-based PC microcavity

Year	Structure	$Q(V)$	Institution
1997	1D PC; one hole removed in a ridge waveguide	265 (V = 0.055 μm^3)	MIT [8]
2003	2D PC; three holes removed, with nearby holes shifted in an asymmetric slab	45,000 (V = 0.07 μm^3)	Kyoto University [9]
2005	2D PC; three holes removed, with nearby holes fine-tuned in an asymmetric slab	100,000 (V = 0.071 μm^3)	Kyoto University [10]
2006	2D PC; fine-tuning periodicity in an asymmetric slab	1,000,000 (V = 1.3 $(\lambda/n)^3$)	Kyoto University [11]
2007	2D PC; heterostructure surrounding microcavity in an asymmetric slab	2,500,000 (V = 1.4 $(\lambda/n)^3$)	Kyoto University [12]

6.5.3 SOI PC Filters

Because of many excellent photonic effects, a lot of devices, such as source, modulator, switch, and detector. have been created in silicon-based PCs. Here we take a channel drop filter [13] as an example to show how we design, optimize, and fabricate such devices.

The channel drop filter is designed in a PC slab with an air-hole triangular lattice, as shown in Fig. 6.12a. The two PC waveguide buses separated by seven row air holes are both W1 waveguides along the Γ*K* direction, and the two symmetric microcavities lying between the parallel waveguides are obtained by removing five air holes in the same direction.

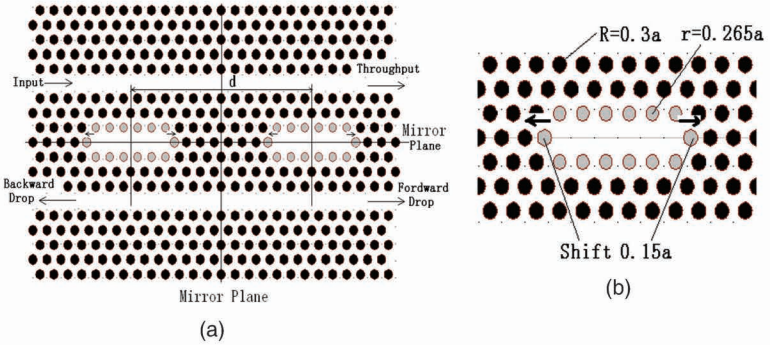

Figure 6.12 (a) Sketch of the optimized PC filter. (b) Structure of the microcavities after optimization.

The radii of the bulk air holes are $\boldsymbol{r} = 0.3\boldsymbol{a}$, where $\boldsymbol{a}$ is 450 nm, representing the lattice constant. Coupling between the two microcavities results in the formation of two coupled cavity modes, and they are even and odd resonant modes, respectively, with respect to the mirror plane perpendicular to the waveguides. To achieve complete channel drop transfer from one waveguide to the other, the bandwidths and resonant frequencies of the coupled cavity modes must be made equal. The bandwidths of the resonances become equal when the following equation or phase matching condition is satisfied [10]:

$$kd = n\pi \pm \pi/2, \tag{6.5}$$

where k is the wave vector at the operating frequency, d is the distance between the two microcavities, and n is an integer number. As can

be seen from Fig. 6.12a, d is chosen to be $13a$. Therefore, k should be $0.5\pi/a$ for $n = 6$. From the dispersion curves of the guided modes in the W1 waveguide shown in Fig. 6.13, which was calculated by using the PWE method, it is seen that the corresponding normalized operating frequency for k of $0.5\pi/a$ is about $\omega = 0.2838(a/\lambda)$, as shown by the y axis coordinate of the working point **A** in Fig. 6.13.

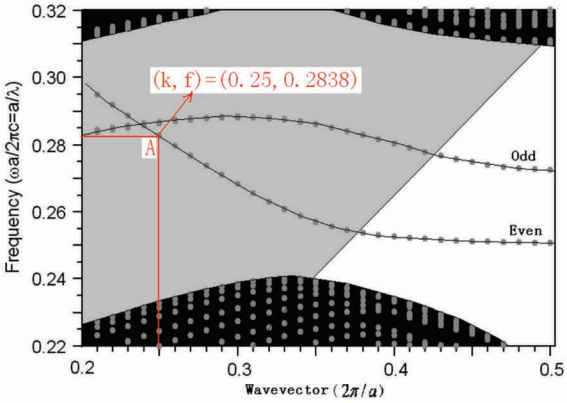

Figure 6.13 The dispersion curves for the guided modes in the W1 waveguide.

To operate the coupled microcavities at the set frequency of $\omega = 0.2838(a/\lambda)$, the cavity structure parameters should be finely tuned. The optimization process was performed by using the 3D FDTD method. The structure of the microcavities after optimization is shown in Fig. 6.12b. It is seen that the radii of the 12 air holes around the defects should be reduced to about $0.265a$ and that the two edge holes of each microcavity should be shifted outward by $0.15a$ from the default positions.

$$1/Q_t = 1/Q_{iso} + 1/Q_c \tag{6.6}$$

The corresponding wavelength is 1585 nm for $\omega = 0.283(a/\lambda)$ and $a = 450$ nm, and FDTD simulations showed that the Q factor of the isolated microcavity (without coupling with the waveguides) was about 4000. The total Q factor of the filter can be evaluated by using Eq. 6.6, where Q_{iso} is the isolated cavity quality factor, and $1/Q_c$ represents the cavity energy loss due to coupling with the waveguides, which can be calculated by FDTD. Then the total Q factor of the filter that determines the bandwidth was estimated to be about 1260. There are mainly two reasons contributing to energy

losses in the microcavities: first, since the working point denoted by A in Fig. 6.13 lies in the light cone of silica, the coupling loss between the resonant modes and the radiation modes in the cladding cannot be avoided. Second, the PC slab is asymmetric, which will result in the coupling of quasi-TE modes and quasi-TM modes in some frequency ranges, and a considerable amount of energy loss arises. If most of the energy losses due to the above mechanisms are suppressed, the total Q factor will be further increased and the maximum can be as high as 15,000, predicted by numerical calculation.

Figure 6.14 shows the electric field $\vec{E}_y$ component in the optimized PC channel drop filter. When the frequency of the input light is off-resonance, the light from port 1 will be transmitted along the W1 waveguide to port 2. However, when the light frequency equals the resonant frequency of the coupled microcavities, the input light will drop to the other W1 waveguide. Since the phase matching equation Eq. 6.20 is satisfied, most of the light will be put out from port 4, as can be seen from Fig. 6.14b. It was calculated that the efficiency of port 4 was about 90%.

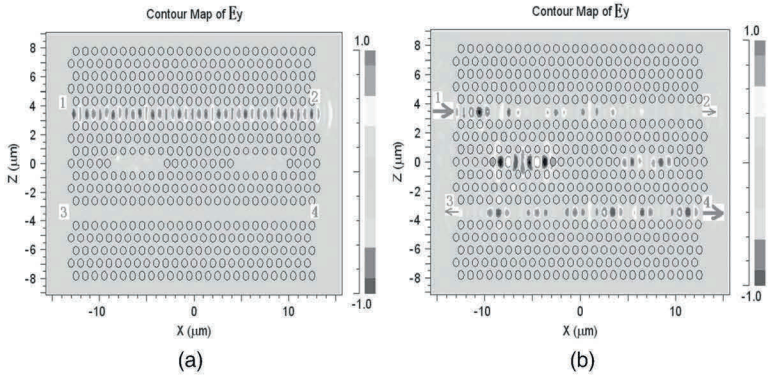

Figure 6.14 3D FDTD-simulated electric field $\vec{E}_y$ component in the PC channel drop filter. (a) Off resonance and (b) on resonance.

The PC filter with the above-optimized parameters was fabricated by electron beam lithography (EBL). First, a 150 nm thick poly(methyl methacrylate) (PMMA) 950 K e-beam resist layer was spun onto a piece of SOI wafer (Soitec Inc.) from a 2% solution in chlorobenzene. The PMMA-layer thickness was chosen in order to avoid electron proximity effect and enable the pattern transfer to the wafer in ICP etching, accounting for the Si/PMMA etching selectivity.

The processing followed the recipe given in Table 6.1. Finally, the wafer was cleaved for measurement and scanning electron microscopy (SEM) characterization.

An SEM image of the central part of the fabricated sample is shown in Fig. 6.15. The access and exit ridge waveguides for measurement are outside the image. It is seen that the air holes have been clearly defined. The air holes were measured to be a little elliptical, which was due to the imperfect adjustment of the EBL system in exposure. The edge roughness of waveguides and air holes is from ±10 to ±20 nm. The above factors lead to a maximum difference of ±10% between the radii of the fabricated and targeted air holes.

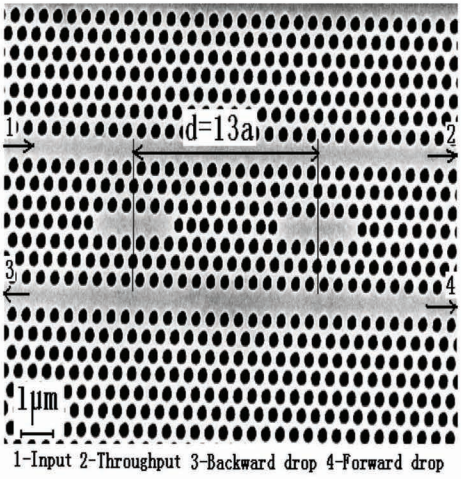

Figure 6.15 An SEM image of the fabricated PC filter on an asymmetric SOI slab.

The transmission spectrum of the sample was measured by using the Newport PM500-C Precision Motion Controller together with the Agilent 8164A Lightwave Measurement System in which a tunable laser (Agilent 81640A), a polarization controller (Agilent 8169A), and a detector unit were integrated. The laser tunable from 1510 to 1640 nm was first modulated to TE-like polarization by Agilent 8169A, which provides polarization synthesis by using a linear polarizer, a quarter-wave plate, and a half-wave plate. The coupling of light with the chip was realized by two identical lensed fibers. The output TE light was selected by a polarizer before it was

sent to the built-in detector to ensure measurement of the correct polarization. Though a part of TE light may convert to TM light in the tapered fibers or in the chip, other polarizations were filtered out and only TE light was detected.

The measured spectrum is illustrated in Fig. 6.16. There is a stop-band around the wavelength of 1550 nm, which is due to the PBG effect in the W1 waveguide. A drop peak with an extinction ratio of 6.3 dB appears at about 1598 nm, demonstrating the filter effect of the coupled microcavity system. The drop efficiency of the filter is about 73% ± 5%, estimated by dividing the peak intensity of the "through spectrum" by the peak intensity of the "transmission spectrum" of a reference W1 waveguide at the same wavelength. The total Q factor of the filter is around 1140, through the estimation of the full width at half maximum of the drop peak fitted by a Lorentz function. Therefore, the measured Q factor is very close to the simulation result of 1260. The position of the measured drop peak is red-shifted about 13 nm compared to the simulated result of 1585 nm, owing to the fabrication imperfections as has been analyzed above.

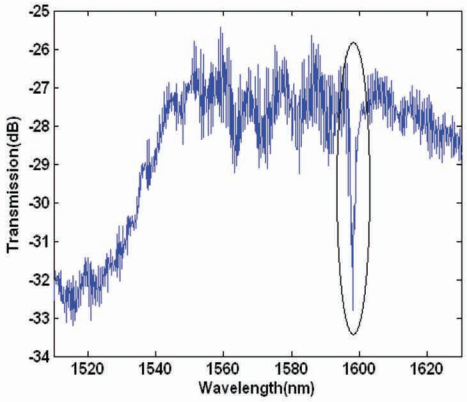

Figure 6.16 The measured spectrum of the filter.

6.6 Conclusions

In conclusion, the basic concepts, calculation methods, fabrication process, waveguides, microcavity, and typical devices of silicon-

based PCs are discussed in this section. The invention of PCs makes it possible to manipulate light on a wavelength scale, and the advanced fabrication process and excellent waveguide characteristics of silicon provide an easier way to discover many interesting physical characteristics of PCs, on the basis of which many useful structures and devices can be created. Therefore, silicon-based PCs may be a good choice to achieve high densities in future high-performance photonic integrated circuits.

Acknowledgments

We thank Hejun Yu and Zhiyong Li for the collection of basic information and figure drawings.

References

1. E. Yablonnovitch (1987). Inhibited spontaneous emission in solid-state physics and electronics, *Phys. Rev. Lett.*, **58**(20), 2059–2062.
2. S. John (1987). Strong localization of photons in certain disordered dielectric superlattices, *Phys. Rev. Lett.*, **58**(23), 2486–2489.
3. K. Sakoda (2001). *Optical Properties of Photonic Crystals* (Springer-Verlag, Berlin).
4. J. D. Joannapolous, R. D. Meade and J. N. Winn (1995). *Photonic Crystal-Molding the Flow of Light* (Princeton University Press).
5. K. S. Yee (1966). Numerical solution of initial boundary value problems involving Maxwell's equations in isotropic media, *IEEE Trans. Antennas Propagat.*, **AP-14**, 302.
6. A. Tavlove (1995). *Computational Electrodynamics: The Finite-Difference Time-Domain Method* (Artech House, Norwood).
7. H. Yu, J. Yu, F. Sun, Z. Li and S. Chen (2007). Systematic considerations for the patterning of photonic crystal devices by electron beam lithography, *Opt. Commun.*, **271**(3), 241–247.
8. J. S. Foresi, P. R. Villeneuve, J. Ferrera, E. R. Thoen, G. Steinmeyer, S. Fan, J. D. Joannopoulos, L. C. Kimerling, H. I. Smith and E. P. Ippen (2003). Photonic-bandgap microcavities in optical waveguides, *Nature*, **425**, 944–947.

9. Y. Akahane, T. Asano, B. S. Song and S. Noda (1997). High-Q photonic crystal nanocavity in a two-dimensional photonic crystal, *Nature*, **390**, 143–145.
10. Y. Akahane, T. Asano, B.-S. Song and S. Noda (2005). Fine-tuned high-Q photonic-crystal nanocavity, *Opt. Express*, **13**(4), 1202–1214.
11. T. Asano, B. S. Song and S. Noda (2006). Analysis of the experimental Q factors (~1 million) of photonic crystal nanocavities, *Opt. Express*, **14**(5), 1996–2002.
12. T. Yasushi, H. Hiroyuki, T. Yoshinori, S. Bong-Shik, A. Takashi and S. Noda (2007). High-Q nanocavity with a 2-ns photon lifetime, *Opt. Express*, **15**(25), 17206–17213.
13. H. Yu, J. Yu, Y. Yu and S. Chen (2009). Design and fabrication of a photonic crystal channel drop filter based on an asymmetric Silicon-on-insulator slab, *J. Nanosci. Nanotechnol.*, **9**, 974–977.